condition [10],

$$k_{\mathrm{SPPgr}} = k_0 \sin\theta + \frac{2m\pi}{d}, \qquad (1)$$

where k_{SPPgr} and $k_0 = 2\pi/\lambda_0$ is the wave vector of SPP at the grating and that of light in free space, respectively, λ_0 is the wavelength of light in free space, θ is an incident angle, d is a grating pitch, and m is a positive or negative integer. Here we note that $k_{mathrmSPPgr}$is close to the SPP wavevector on a flat film in the case of shallow gratings and does not vary much with grating geometry.

Grating depth is known to be significantly influential for the light-SPP (or SPP-light) coupling efficiency[10][11]. To find the optimum grating height for the strongest coupling, we conducted numerical simulations on reflection efficiencies of surface relief gratings made of gold, based on rigorous coupled-wave analysis (RCWA)[12].

Here, we assumed that each grating is made of polycrystalline gold (E. D. Palik, Handbook of Optical Constants of Solids (Academic Press, Orlando, 1985)) with a rectangular profile, a grating pitch of 15 μm, and a duty cycle of 0.5. We also assumed that incident light is a plane monochromatic wave with a wavelength of 10.6 μm. Figure 1(b) shows the calculated reflection efficiency as a function of incident angle and grating depth. The reflection efficiency shows a dip at the grating depth $0.2 - 1.3$ μm for the incident angle of 17-18 degree. The loss of power in the reflected beam originates from energy conversion from propagating lights in free space to SPPs. Here we set the grating period and the incident angle so as to minimize power loss into diffracted light in free space; there is no diffraction other the specular reflection and an SPP propagating in uni-direction. From these numerical results and the possible beam divergence (?degree) of the incident light in our experiments, we predict that efficient coupling would be obtained for the grating depth of ~ 0.8 μm. This prediction is consistent with a previous report which concluded that the optimum grating depth of a rectangular grating is 10%-15% of the wavelength in mid-infrared range[11].

Figure 1(c) shows the design of the waveguide devices. The waveguides have a common width of 0.5 mm and varied lengths of $3, 5, 7, 9, and 11$ mm. The input (output) coupler is 1 mm in length and 0.5 mm (1.5 mm) in width. Both of the input/output couplers have rectangular profiles with a grating pitch of 15 μm and a duty cycle of 0.5. As will be described below, both of the waveguides and the grating structures arefabricated on a 200-nm-thick gold evapolation film, and are 0.8 μm in hight.

The device was fabricated by means of electron beam lithography, thermal evaporation, and lift-off process. Gold base layer with a thickness of 200 nm was thermally evaporated on a silica glass substrate with a 5-nm-thick chromium adhesion layer, after the substrate was cleaned with acetone and ethanol. Then, electron-beam resist (OEBR-CAP112PM, Tokyo Ohka Kogyo Co., Ltd) was spin-coated with a thickness of 1700 nm on the gold base layer, exposed by electron beam, and developed. Finally, gold with a thickness of 800 nm was deposited on the developed resist, and the resist was lifted off by acetone. The whole fabrication process was conducted at room temperature. During the evaporation, we maintained the evaporation rate of gold to be 0.4 nm/s, and the pressure inside the vacuum chamber to be less than 3×10^{-5} Torr.

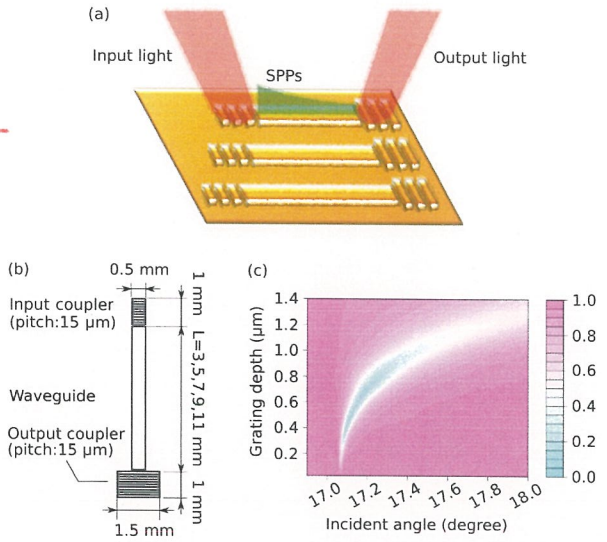

Figure 1: (a) Schematic of the SPP device. (b) Calculated reflection efficiency of a gold relief grating with a grating pitch of 15 μm and a duty cycle of 0.5, as a function of the incident angle and the grating depth. (c) Design of SPP waveguide and input/output couplers. THE ORDER HAS BEEN CHANGED!

used in this study.

3 Experiment

Figure ?? shows the schematic of our experimental setup. A CO_2 laser was used as a mid-IR light source generating linearly polarized light at a wavelength of 10.6 μm. The SP device was attached to a rotational and xyz-translational stage. P-polarized light was incident onto the input coupler at a certain angle that fulfills Eq. 1 where $m = 1$, being loosely collimated by a spherical mir-

ror with a radius of curvature $R = 400$ mm. Here the incident light converges with an angle as small as ? degree. This plane-like wavefront of the incident light and the homogeneous grating coupler results in a collimated SPP beam which should propagate with low divergence. The SPP beam divergence is extimated to be ? degree and therefore we believe that the excited SPP beam propages freely along the waveguide without horizontal confinement owing to the SPPwaveguide. The output light was collected by a spherical mirror of $R = 150$ mm and a power meter. An aperture was placed at the conjugate point of the output coupler. The time averaged power of the CO_2 laser was controlled by changing the duty ratio of the RF power modulation. The optical power sent to the input coupler was typically 60 mW, and the duty ratio was typically 0.5. We also used a He-Ne laser as a guide laser, which was collinearly overlapped with the mid-IR light.

In order to modify the morphology of the gold film, the sample was annealed twice with a hotplate in Argon atmosphere[13]. In the first annealing process, the sample was heated at 600 °C for 20 min., and gradually cooled on the hotplate to room temperature. In the second annealing process, the sample was heated at 700 °C for 16 min., and cooled down in the same way.

Surface morphology was measured by AFM in non-contact mode (DESCRIBE THE PRODUCT NAME AND THE PRODUCTION COMPANY OF THE AFM), and crystal grains were identified by analyzing the height data of the surface based on the watershed algorithm[14].

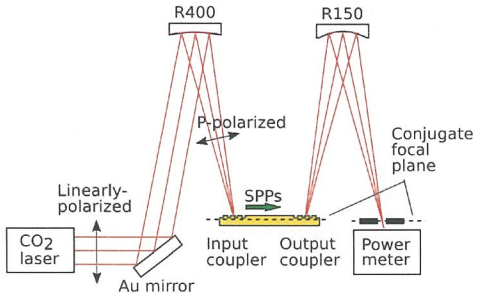

Figure 2: Schematic of experimental setup.

4 Results

Figure 3 shows the measured output power as a function of the SPP waveguide length L for (a) the as-grown, (b) once-annealed (600 °C), and (c) twice-annealed (600 °C and 700°C) sample. Here, each trace ($a \sim c$) of the output power is normalized by the value at $L = 0$ obtained by the least squares fitting with the exponential decay function $\exp(-L/L_{\mathrm{SPP}})$. The propagation length L_{SPP} is evaluated as 9.0±0.3mm, 12.0±0.4mm, and 14.7±0.7mm for the sample (a), (b), and (c), respectively. In this way, the propagation length increased by the annealing process.

The SPP-light coupling efficiency of the grating is estimated to be 18% in the experiment, by calculating a square root of the normalized output power at $L = 0$ divided by the input power. After annealing, optimum incident angle for the maximum excitation efficiency of SPP was shifted by about 0.5°, but no significant change was confirmed in the value of the efficiency.

Figure 4 shows AFM topography images of the surface of SPP waveguides for the sample (a), (b), and (c). Isotropic deposition of gold and flat surface were confirmed for all samples.

Surface roughness is estimated to be 5.67 nm, 2.82 nm, and 2.15 nm for the sample (a), (b), and (c), by calculating two-dimensional root mean squares of deviations in height data. The surface roughness decreased by the annealing process.

For detailed characterization of the surface morphology, crystal grains were identified based on the watershed algorithm. Aspect ratio of the grain is calculated as 1.6±0.8, 2.4±2.5, and 2.0±1.8 for the sample (a), (b), and (c), respectively. In the assumption that the grains are close to spherical shape, grain diameter is estimated to be 70 nm, 190 nm, and 180 nm, for the sample (a), (b), and (c), respectively. In this way, the crystal grain size significantly increased by the first annealing at 600 °C, and remained similar by the second annealing at 700 °C.

The grating structures were not significantly deformed after the annealing. However, pinholes with diameters of $0.3 - 1.2$ μm appeared with a number density of $0.16\,\mu\mathrm{m}^{-2}$ after the first annealing process, and increased to $0.44\,\mu\mathrm{m}^{-2}$ in number density after the second annealing.

5 Discussion

Propagation length of SPP L_{SPP} at Au/air boundary can be calculated by the following equation,

$$L_{\mathrm{SPP}} = \frac{1}{2\,\mathrm{Im}k_{\mathrm{SPP}}}, \qquad (2)$$

where the wave vector is $k_{SPP} = \lambda/(2\pi\sqrt{\epsilon_g/(\epsilon_g+1)})$, and $\epsilon_g = \epsilon_g' + i\epsilon_g''$ is relative dielectric constants of gold. By substituting the dielectric constant of polycrystalline gold[15] into Eqn. 2, the propagation length of SPP is calculated to be 12.3mm at a wavelength of 10.6μm. Our

mid-IR SPPs at gold/air interface propagates for a distance as long as > 10 mm.

experimentally measured values of 9.0 ± 0.3 mm, 12.0 ± 0.4 mm, and 14.7 ± 0.7 mm agree with the theoretical estimation of 12.3 mm, confirming that SPPs at Au/air interface do propagate for along distance of > 10 mm.

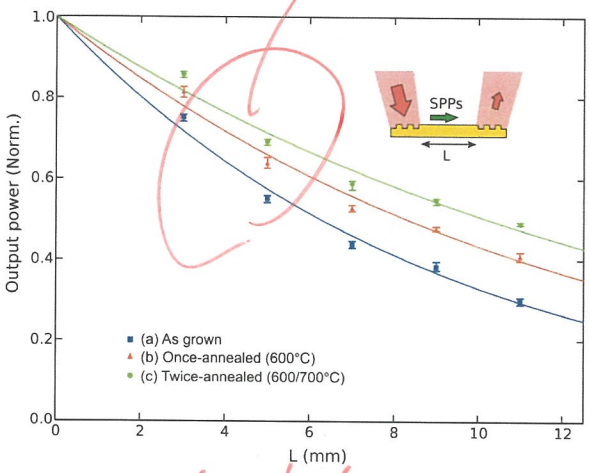

Figure 3: Measured output power as a function of the SPP waveguide length L for (a) the as-grown, (b) the once-annealed (600 °C), and (c) the twice-annealed sample (600 °C and 700 °C). The propagation length of SPP is evaluated as 9.0 ± 0.3 mm, 12.0 ± 0.4 mm, and 14.7 ± 0.7 mm, respectively for the sample (a), (b), and (c).

Grain boundaries reduce the mean free path of electrons[7]. Therefore, the SPPs loss its energy by introduction of the grain boundaries due to the oscillating electrons, decreasing the propagation length. An additional loss mechanism was suggested in [16], that SPPs scatter due to inhomogeneities of free electron gas due to grain boundaries.

Comparing the first annealing at 600 °C , we find enlargement of the crystal grains, suppression of the surface roughness, and the increased propagation length. Since influence of the grain boundaries become stronger as the averaged grain diameter decreases, we confirmed the longer propagation length of the mid-infrared SPPs in mid-infrared range which is contributed from enlargement of crystal grains.

After the second annealing at 700 °C, although the propagation length increased considerably, the averaged grain diameter does not enlarged, comparing the once-annealed sample and the twice annealed sample. This mismatch occurred can be attributed to the reduced aspect ratio of the crystal grains and the deviation. As the aspect ratio decrease, the area of grain boundaries get smaller even if the estimated grain diameter was unchanged. It follows that, averaged number of grain boundaries that the SPPs passing through per a unit length increases, and the mean free path of electron decreases. The reduced deviation results similarly to the area of grain boundaris, thus influences the mean free path of electrons. In any case, the elongated propagation length was demonstrated by the annealing, which is relevant with the material morphology.

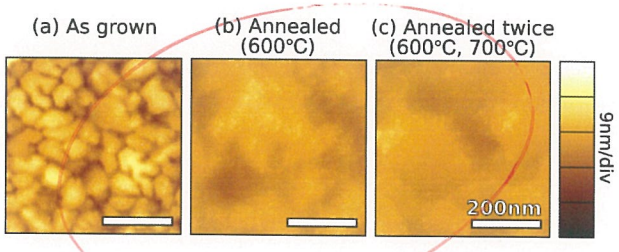

Figure 4: Height plots on the surface of waveguides based on AFM.

Thermal annealing is convenient method for controlling material morphology[13]. Its minor side effects are that pinholes were generated on the surface of waveguides by the annealing. However, the propagation length increased by the annealing, and the the size of the pinhole is much smaller than the wavelength of the mid-infrared SPPs. Therefore we conclude that the decrease of the propagation length due to the pinholes is less than the increase of the propagation length due to the morphology change. Moreover, the optimum incident angle onto the gratings was shifted by about 0.5°. This angle shift is supposed to be slightly different for each of the gratings, resulting in the increased relative error for the measured propagation length.

As presented above, we showed that SPPs at Au/air interface propagates as long as > 10mm at the mid-infrared wavelength of 10.6 μm. We also demonstrated that the SPP propagation length increase by thermal annealing,

In the following, we will discuss the reasons why the propagation length increased by thermal anneal.